

available at www.sciencedirect.comjournal homepage: www.elsevier.com/locate/jmbbm

Research paper

Robustness and optimal use of design principles of arthropod exoskeletons studied by *ab initio*-based multiscale simulations

S. Nikolov^a, H. Fabritius^b, M. Petrov^b, M. Friák^b, L. Lymparakis^b, C. Sachs^c,
D. Raabe^{b,*}, J. Neugebauer^b

^aBulgarian Academy of Sciences, Institute of Mechanics, Acad. G. Bonchev Str. Bl. 4, 1113 Sofia, Bulgaria

^bMax-Planck-Institut für Eisenforschung GmbH, Max-Planck-Str. 1, 40237 Düsseldorf, Germany

^cMassachusetts Institute of Technology, 77 Massachusetts Avenue, Building 35-135A, Cambridge, MA 02139-4307, USA

ARTICLE INFO

Article history:

Received 28 February 2010

Received in revised form

16 September 2010

Accepted 27 September 2010

Published online 1 October 2010

Keywords:

Chitin

Biomaterials

Elastic properties

Ab initio method

Homogenization

ABSTRACT

Recently, we proposed a hierarchical model for the elastic properties of mineralized lobster cuticle using (i) *ab initio* calculations for the chitin properties and (ii) hierarchical homogenization performed in a bottom-up order through all length scales. It has been found that the cuticle possesses nearly extremal, excellent mechanical properties in terms of stiffness that strongly depend on the overall mineral content and the specific microstructure of the mineral–protein matrix. In this study, we investigated how the overall cuticle properties changed when there are significant variations in the properties of the constituents (chitin, amorphous calcium carbonate (ACC), proteins), and the volume fractions of key structural elements such as chitin–protein fibers. It was found that the cuticle performance is very robust with respect to variations in the elastic properties of chitin and fiber proteins at a lower hierarchy level. At higher structural levels, variations of design parameters such as the volume fraction of the chitin–protein fibers have a significant influence on the cuticle performance. Furthermore, we observed that among the possible variations in the cuticle ingredients and volume fractions, the experimental data reflect an optimal use of the structural variations regarding the best possible performance for a given composition due to the smart hierarchical organization of the cuticle design.

© 2010 Elsevier Ltd. All rights reserved.

1. Introduction and motivation

Most biological materials with structural functions in the animal kingdom consist of an organic matrix of structural biopolymers like collagen and chitin which is modified and reinforced with different proteins and in many cases also

with biominerals. The most prominent examples of such materials, like the bones of vertebrates, the exoskeletons of arthropods, and mollusk shells, are known to possess excellent mechanical properties (e.g., in terms of stiffness-to-density ratio and fracture toughness). The origins of these properties have become the subject of intensive research in

* Corresponding author.

E-mail address: d.raabe@mpie.de (D. Raabe).

recent years (Vincent, 1990; Currey, 1996; Weiner and Addadi, 1997; Vincent and Wegst, 2004; Ashby and Wegst, 2004; Tai et al., 2007; Buehler and Wong, 2007; Ortiz and Boyce, 2008; Chen et al., 2008; Meyers et al., 2008; Al-Sawalmih et al., 2008; Fabritius et al., 2009). It has been observed that the specific design and properties at the nanoscale contribute significantly to their macroscopic properties (Nikolov et al., 2010). Evidently, the overall properties depend on the specific microstructure at all levels of hierarchy. However, in particular, the properties at small length scales are experimentally hard, if not impossible, to access due to methodological constraints. Hence, multiscale modeling that can systematically describe and investigate materials properties from the atomistic scale up to the macroscopic level has become a major approach to tackle the structure–property relations of biological organic/inorganic nanocomposites and has been applied to bone, mother of pearl, lobster cuticle, and related heterogeneous natural compounds (see, e.g., Vincent and Wegst, 2004; Ashby and Wegst, 2004; Raabe et al., 2005, 2006; Fratzl and Weinkamer, 2007; Nikolov and Raabe, 2008). In addition to modeling fully differentiated structural composites, the approach has been successfully applied to model the mechanical properties of individual constituents and to explain the structure–property relations on increasingly complex structural hierarchy levels. For non-mineralized soft tissues, important work on collagen fibril and tissue mechanics based on a multiscale approach linking molecular to continuum scales (Buehler, 2008; Tang et al., 2009) showed that there is a strong dependence of the fibril (tissue) response on nanoscopic structural features such as the density of crosslinks between neighboring collagen molecules.

Most multiscale models use fixed averaged values for the properties and volume fractions of the constituents (structural polymers, proteins, minerals) to predict the overall tissue properties. However, in reality, due to structural variations such as caused by different stages of growth, molt cycle, injuries, and synthesis heterogeneity, the properties and the volume fractions of the tissue constituents may vary considerably locally. Thus, an important question is how much the overall tissue properties change upon such structural variations of the building blocks on the small length scale. Tackling this question helps to better understand the robustness of biological tissue design. Experimentally validated physics-based multiscale models are an excellent vehicle to conduct such structure–property tolerance studies as the different ingredients and their behavior can be systematically varied. In a very recent work, a similar sensitivity analysis using multiscale modeling has been applied to bone (Reisinger et al., 2010).

The fact that the structure and mechanical properties of some constituents in biological hard tissues (e.g., proteins) are not well understood at present suggests an additional benefit of theory-assisted structural design analysis. It is therewith possible to identify at least the most probable order of magnitude of some of their properties by the comparison of corresponding multiscale predictions with experimental data.

A similar question arises with respect to biomimetic considerations. The aim of reproducing certain properties of biological matter in a synthetic material does not necessarily

require copying the original biological structure but rather understanding the mechanical principle behind the material and replacing the underlying building blocks or their topological connectivity. A corresponding multiscale modeling approach can help to identify the relevant key ingredients with respect to a certain property and the tolerance of the overall material behavior against structural variations. We also address that current experimental observations suggest that among a set of possible structural variations real biological materials often reveal an optimal use of their ingredients regarding the best possible performance for a given composition.

In this work, we investigated these two questions of structural tolerance and optimal use taking mineralized load-bearing parts of the chitin-based exoskeleton of the crustacean *Homarus americanus* as a case study. The exoskeletons of all Arthropoda are formed by the cuticle which covers the entire animal and is locally modified in microstructure and chemical composition to perform all the functions required to meet the ecophysiological strains encountered by the organism. The cuticle represents a multilayered chitin–protein-based composite whose microstructure is hierarchically organized (Fig. 1). On the low levels of structural hierarchy, this general scheme appears to be valid for all arthropods. On the higher levels, significant differences can be found both in structural organization and in chemical composition between different taxa and even in closely related species (Neues et al., 2009; Hild et al., 2008, 2009). Crustaceans, for instance, reinforce the hard, load-bearing parts of their cuticle by incorporating various biominerals. The shell of the American lobster contains variable amounts of amorphous (ACC) and crystalline (calcite) calcium carbonate (Boßelmann et al., 2007).

The lowest level of hierarchy in the general arthropod model is represented by acetylglucosamine molecules (I) which polymerize to form chains of chitin (II). At the next hierarchy level (III), 18–25 chitin molecules arrange anti-parallel to form crystalline α -chitin nanofibrils with a diameter of about 3 nm. Each nanofibril is individually wrapped with proteins. Next, the chitin–protein nanofibrils cluster to form chitin–protein fibers (IV) with diameters \sim 20 nm. In the plane of the cuticle, the mineralized chitin–protein fibers are arranged in planes with roughly parallel orientation of their long axes (V). In *H. americanus*, level V is formed directly by chitin nanofibrils arranged in horizontal planes. The arrangement is interrupted by voids originating from the pore canal system whose original function is to enable transport of minerals after molting, the process where arthropods replace their old exoskeleton with a new, larger one in order to grow. Hence, the resulting tissue appears as a honeycomb-like structure (V*). At this level, nanoscopic calcium carbonate particles become embedded in the protein matrix of the nanofibrils. The individual chitin–protein fiber planes (V) or nanofibril planes in case of our lobster (V*) are stacked over each other and gradually rotate around the normal direction of the cuticle, which results in a twisted plywood (Bouligand) structure (VI) pierced by pore canals in the form of twisted ribbons with elliptical cross section. At the macroscopic scale (VII), the cuticle consists of three layers: endocuticle, exocuticle, and an outer thin waxy layer, the epicuticle. The mechanically relevant exocuticle and endocuticle share the same

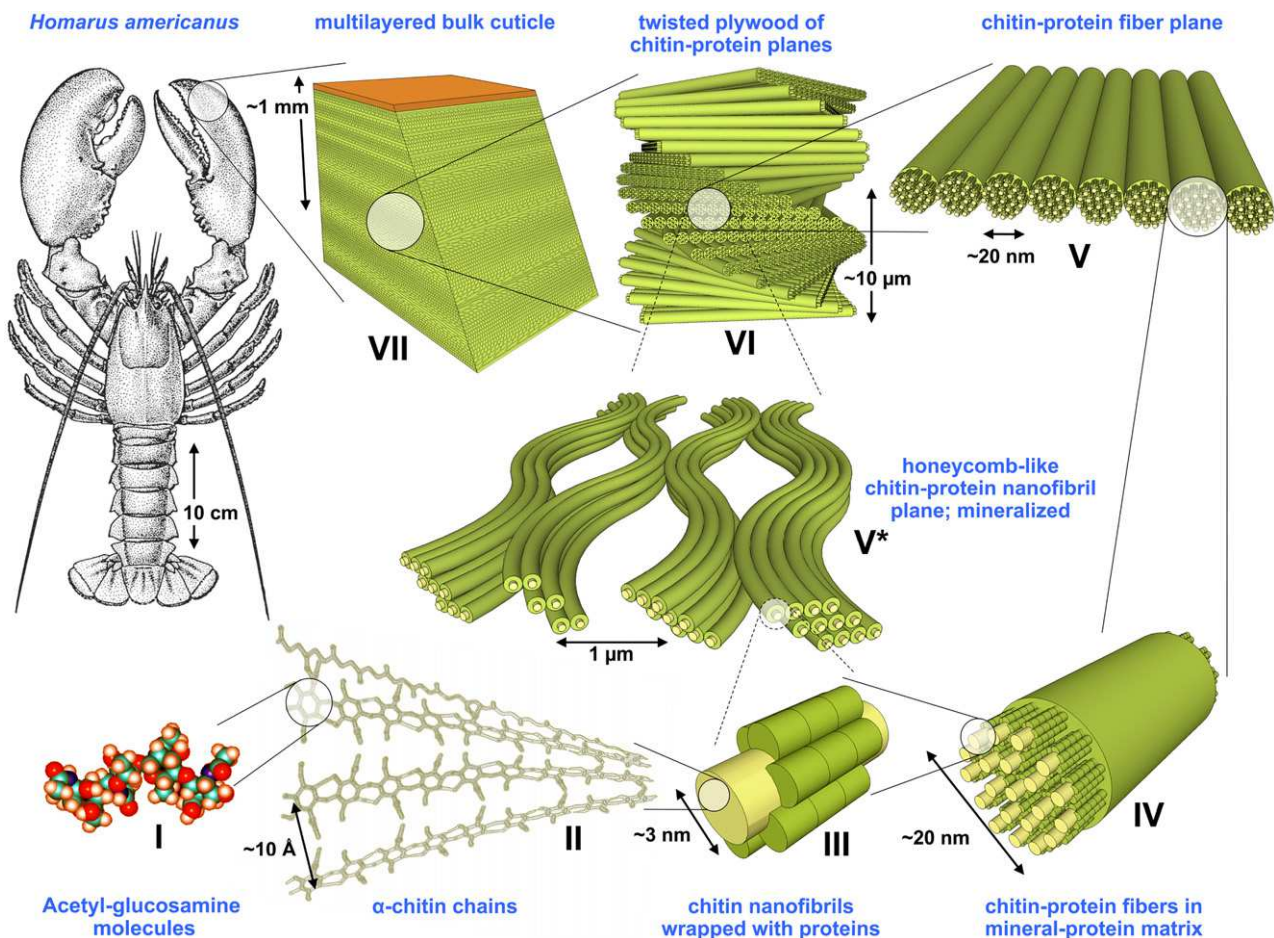


Fig. 1 – Structural hierarchy in arthropod cuticle. Levels I to VII represent the general model assumed for the organic matrix in the cuticle. In *H. americanus*, level IV is not found; the fiber planes are formed already by the protein-wrapped nanofibrils and show a characteristic arrangement due to the well-developed pore canal system giving the resulting bulk a honeycomb-like appearance (V*). Mineralization is not shown.

basic microstructure, but the mineral content in the exocuticle is higher, the pore canals are smaller, and the pitch of rotation of the chitin–protein fiber planes is also smaller compared to the endocuticle (Sachs et al., 2006).

We use our recently proposed multiscale model (Nikolov et al., 2010) for the elastic properties of lobster cuticle to evaluate the robustness and sensitivity of the overall cuticle properties with respect to variations in the properties and the volume fractions of its building blocks (specifically chitin, amorphous calcium carbonate, and the proteins within (i) a single chitin–protein fiber and (ii) the mineral–protein matrix) throughout all relevant scales.

2. Hierarchical modeling approach

The hierarchical model of the cuticle is schematically depicted in Fig. 2. The overall properties are obtained via repeated step-by-step homogenization from the lowest to the highest levels of structural hierarchy. The main goal is to obtain the overall elastic constants of the cuticle, a fundamental characteristic of any heterogeneous body, as a function of the underlying hierarchically organized microstructure. The

information passed from lower to upper hierarchy level of the model in a ‘handshaking’ manner are the elastic constants of the structure at the lower level. For example, the elastic constants of chitin (obtained via molecular dynamics (MD) simulations, levels I and II) are directly introduced in a continuum-scale model to find the elastic constants of chitin–protein fibers (level IIIa). As the properties and the structure of virtually all cuticle proteins are not known, they are assumed to have isotropic properties which are identified via a combined approach using (continuum-scale) modeling and experimental data, as described below.

2.1. *Ab initio* calculations of the ground-state structure and elastic constants of crystalline α -chitin

In nature, chitin adopts three different crystalline forms: α , β , and γ . All three allomorphs are composed of polysaccharide chains of [(1–4)-2-acetamido-2-deoxy- β -D-glucan], and only the mutual orientation of the chains differentiates between them. α -chitin (see Fig. 3) is formed by antiparallel chains whereas the β -chitin consists of parallel ones. The γ crystal is an α – β mixture (Lotmar and Picken, 1950; Carlström, 1957; Rinaudo, 2006; Merzendorfer, 2006).

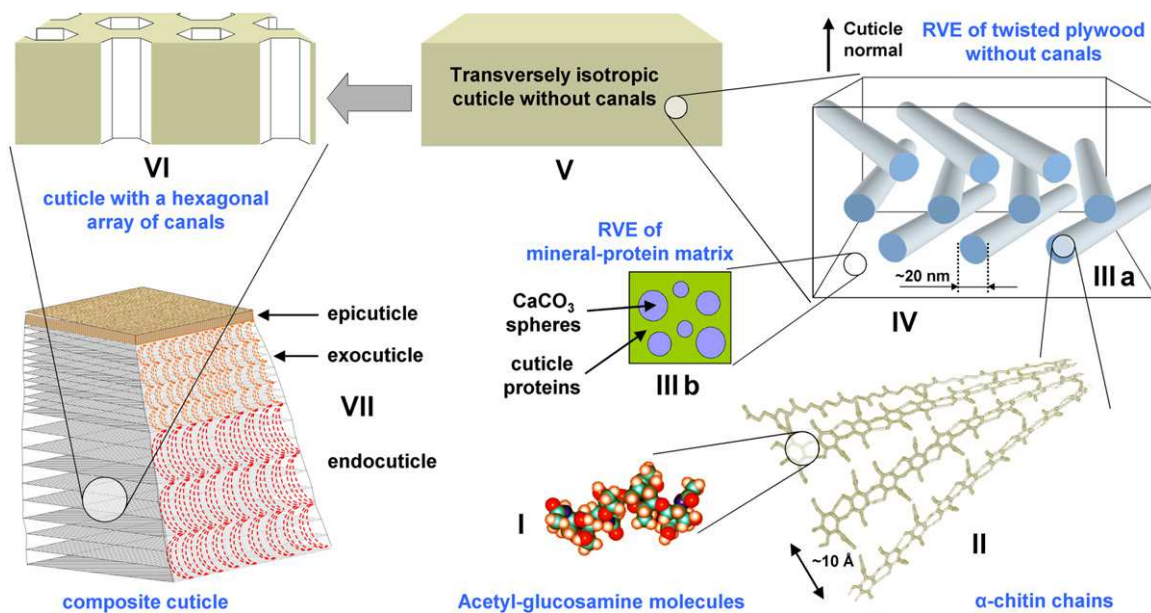


Fig. 2 – Schematic representation of the hierarchical modeling. I, II: chitin properties via *ab initio* calculations; IIIa: single chitin–protein fiber (Mori–Tanaka model); IIIb: mineral–protein matrix (3D Torquato approximation); IV: chitin–protein fibers arranged in twisted plywood and embedded in mineral–protein matrix (combined Mori–Tanaka and Voigt model); V: homogenized twisted plywood without canals; VI: homogenized plywood pierced with hexagonal array of canals (combined 2D Torquato and Voigt model); VII: three-layered cuticle.

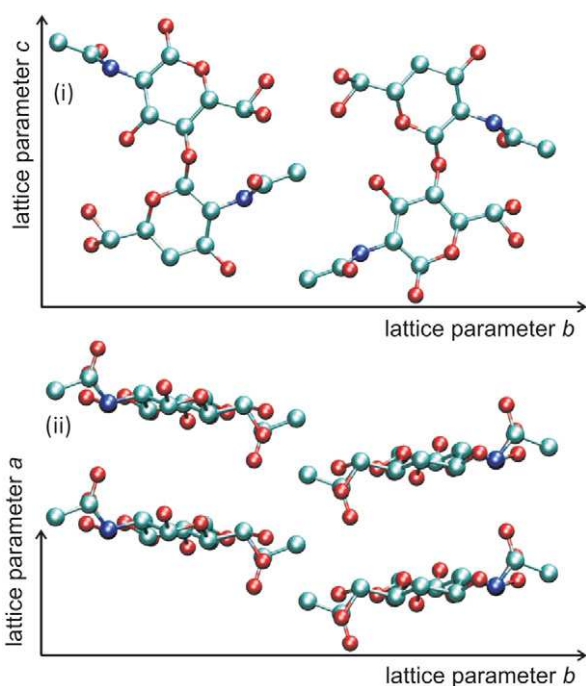


Fig. 3 – The structural model of the crystalline α -chitin, from Minke and Backwell (1978). Oxygen atoms are depicted in red, nitrogen atoms in blue, and carbon atoms in cyan. The length, orientation, and position of the arrows define the unit-cell parameters a , b , and c , used in the *ab initio* calculations. (For interpretation of the references to colour in this figure legend, the reader is referred to the web version of this article.)

The identification of the full atomic geometry of biomolecules by means of atomistic calculations is a challenging task. The presence of an extended hydrogen bond network and the biomolecule structure itself results in high structural flexibility, and subsequently in a large conformational variability: in the case of crystalline α -chitin, the exocyclic side chains ($-\text{OH}$, $-\text{CH}_2\text{OH}$, and $-\text{NHCOCH}_3$) are expected to be prone to conformational changes. Therefore, α -chitin is characterized by a rather complex Born–Oppenheimer (BO) surface with respect to the atomic geometries within which many local minima appear corresponding to different metastable structures. Moreover, the positions of the hydrogen atoms (and consequently the hydrogen bonds) are not easily accessible experimentally. Consequently, they are not known, and thus they enter as variables that must be determined by our simulations. Hence, an approach is required which is able to (i) map a large part of the α -chitin conformational space and (ii) accurately describe the region around the potential energy minimum. Therefore, in order to explore the complex BO surface and investigate the ground-state atomic geometry of crystalline α -chitin, we have employed a hierarchical approach which combines empirical force field molecular dynamics (EFF-MD) (Jensen, 1999) calculations with self-consistent density functional tight binding (SC-DFTB) (Elstner, 2006) and density functional theory (DFT) (Hohenberg and Kohn, 1964; Kohn and Sham, 1965) calculations.

2.1.1. Molecular dynamics simulations

In the first step, the EFF-MD simulations were performed within the framework of a probabilistic conformational search (see Nardi and Wade, 1999, and references therein). Starting from a rather arbitrary conformation of α -chitin

that conserves the chemical formula, an extended MD run was utilized to sample the BO surface. The initial atomic geometry was obtained by using a molecular builder. The chair conformation was chosen for the pyranoid ring while no specific side-chain conformations or any glycosidic bond geometry were promoted. The choice of the size and shape of the periodically repeated unit cell of the initial geometry was based on the X-ray crystallographic data by Minke and Backwell (1978). The MD simulations were performed within the isobaric–isothermal (NPT) ensemble at standard thermodynamic pressure and room temperature. Room temperature was chosen as it was found to be neither too low to trap our search path close to or directly in a local minimum of the BO surface, nor to be too high to result (i) either in disintegration of the structure or (ii) in a non-representative sampling of the conformational space. The advantage of the NPT ensemble is that it allows for variations of the unit cell volume. Thus, it permits one to sample not only the conformational phase space associated with the atomic positions but also the nine degrees of freedom corresponding to all three lattice constants of the orthorhombic unit cell of crystalline α -chitin. For the description of the interatomic interactions we have used the universal force field (UFF) parameterization (Rapp et al., 1992).

The MD calculations are used to generate a stochastic but nevertheless representative set of the conformational space of crystalline α -chitin. Based on the criteria of (i) minimum potential energy and (ii) maximum number of hydrogen bonds, a group of approximately 10^2 out of 10^5 structures emerged from the probabilistic conformation search.

2.1.2. Tight binding—adiabatic approach

In the subsequent level of our hierarchical approach the thus chosen configurations have been refined employing self-consistent density-functional-based tight binding (DFTB) calculations. With respect to the accuracy and computational cost, TB calculations present an intermediate level between (i) the computationally fast but less accurate EFF-MD calculations and (ii) very accurate but computationally expensive DFT calculations. Thus the DFTB calculations serve as a bridge that links the two outermost levels within the hierarchical approach.

The set of $\sim 10^2$ structures identified in the probabilistic conformational search were analyzed in terms of the potential energy as well as the hydrogen bond network. Initially, the structures corresponding to different values of a certain lattice constant were generated in a rather uncontrolled manner: starting from a single conformation as derived from the MD level and dictating different values of the lattice parameters with a step equal to 1% of the initial lattice constant, a number of different structures were generated in parallel by optimizing the internal atomic coordinates for each value of the lattice parameter. However, due to the high structural flexibility of the side chains, the calculated points do not follow a smooth curve, but they resemble a rather scattered behavior. A representative example of the aforementioned behavior is depicted by the filled circles in Fig. 4(a). As can be clearly seen, the energies do not follow a smooth curve with a single minimum.

In order to overcome the problem of the large number of shallow local minima due to highly flexible side chains, we employ an adiabatic/quasi-static approach. Instead of starting the structural optimization from a single conformation for the whole range of lattice parameters and calculating all the data points independently and in a parallel manner, a serial (adiabatic) two-step approach has been adopted. First, a small change of the lattice parameter is made, and the structure is optimized for this slightly altered lattice by minimizing the total energy. Second, the thus optimized atomic coordinates were used as a starting configuration for the next small change of the lattice parameter. The advantage of the adiabatic approach is that the two subsequent structures are structurally close. Thus the system is expected to evolve within the same conformation and within the same potential energy valley over a wide range of lattice constant deformations.

An example of this approach is shown in Fig. 4(a). For clarity, we focus on three points of the energy versus lattice deformation curve obtained within the probabilistic approach that are denoted by the arrows (1)–(3). At each point, two adiabatic paths are followed, corresponding to compressive and tensile strain deformations (Fig. 4(b)–(e)). Applying this approach until convergence resulted in smooth energy over lattice deformation curves. We note that, even within the adiabatic approach, conformational transitions may occur. These transitions correspond to abrupt energy changes of the adiabatic deformation paths in Fig. 4(b)–(d).

In order to understand the atomistic origin of the metastable minima in the total energy landscape, we focus on the sharp step in Fig. 4(b). The corresponding ball and stick models along with the hydroxymethyl $-\text{CH}_2\text{OH}$ side groups which are responsible for the conformational transition are shown in Fig. 5. The hydroxymethyl side groups form rotational conformers (rotamers) which are responsible for the formation of the complex intra-molecular and inter-molecular hydrogen bond pattern. This group is found to be the most flexible part of the structure and to exhibit the highest rotational freedom among all α -chitin side-chain moieties. As shown in Fig. 5(a) and (b), even tiny changes of the a lattice constant of 0.05 \AA can result in abrupt rotations of the hydroxymethyl groups, indicated as (1)–(3). Due to these rotations and the corresponding change in the hydrogen bond pattern, a transition to a neighboring conformational state takes place, accompanied by an abrupt decrease in the potential energy.

Although there is essentially no proof that the state with the minimum potential energy corresponds to the ground state of the conformational space, the simulation of a representative set of different conformations, as emerged from the first step of our hierarchical approach, guarantees that the calculated ground state is very close to the actual ground state.

2.1.3. DFT calculations

The ten lowest energy structures identified in the DFTB calculations were used as input to the subsequent *ab initio* calculations. The latter were performed within DFT using the Perdew–Burke–Ernzerhof generalized gradient approximation (PBE-GGA) for the exchange–correlation functional (Perdew

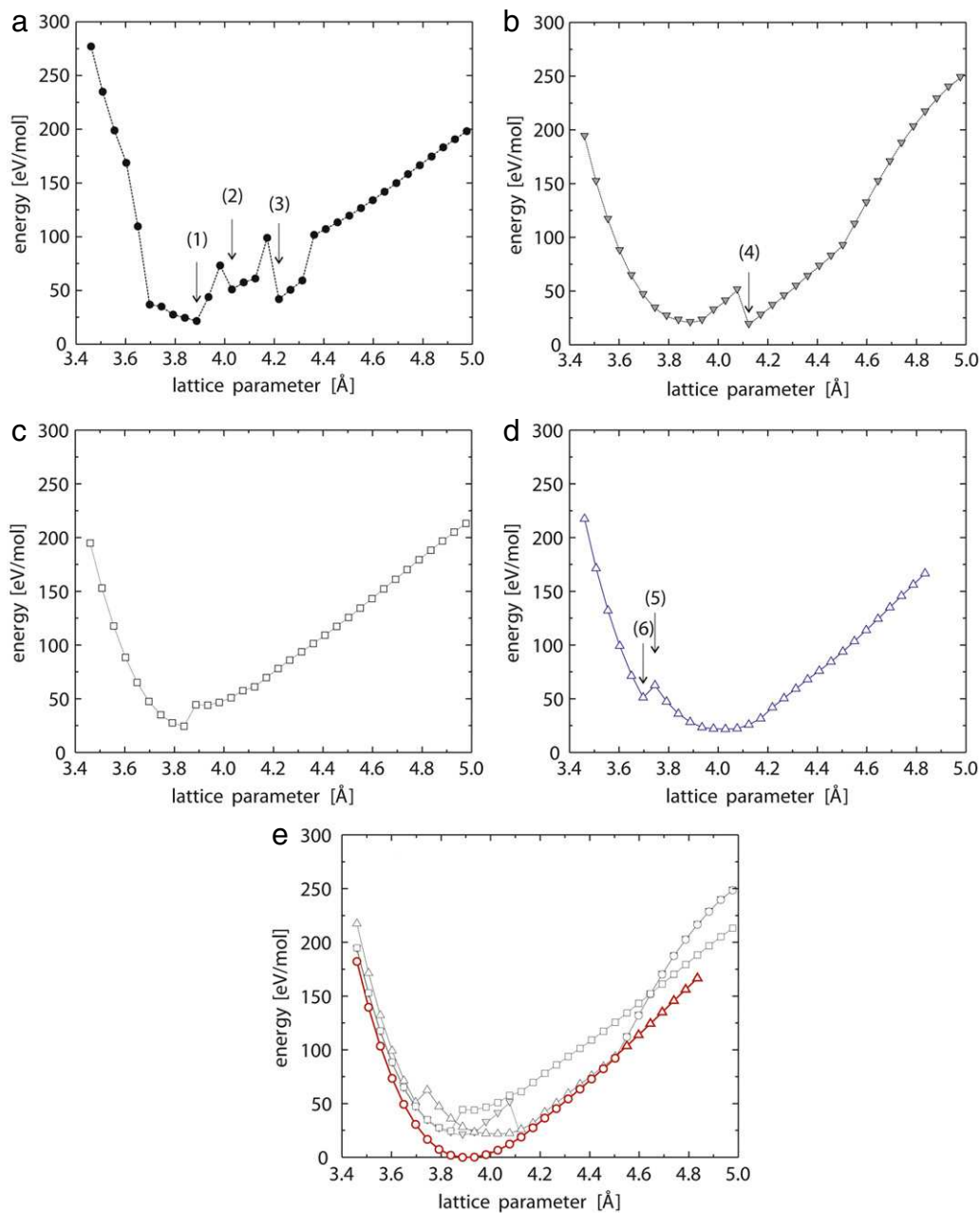


Fig. 4 – Potential energy changes with respect to deformations of the a lattice constant; the b and c lattice constants are kept fixed at 19.237 Å and 10.32 Å, respectively. Filled circles in part (a) correspond to the probabilistic, i.e., non-quasi-static, deformation. The three arrows ((1)–(3)) indicate the starting points for the three quasi-static (adiabatic) deformations (parts (b)–(d)). Filled triangles (part (b)) denote the quasi-static path starting from point (1), open squares (part (c)) the path starting from point (2), open triangles (part (d)) the path starting from point (3), and open circles (part (e)) to the path starting from point (4).

et al., 1996). The electron wave functions were expanded in a plane-wave basis set using 70 Ry cut-off energy, and soft Troullier–Martins pseudopotentials (Troullier and Martins, 1991) have been used. The Brillouin zone was sampled by a $1 \times 2 \times 4$ Monkhorst–Pack mesh (Monkhorst and Pack, 1976). The quasi-static approach described in the previous paragraphs was also employed in this step.

2.2. Homogenization methods

After identifying the ground-state structure and its elastic properties at the atomistic scale, the elastic parameters determined are transferred upscale, taking into account experimental information about the actual composite hierarchy (Fig. 1) reflected in the multiscale structural model used

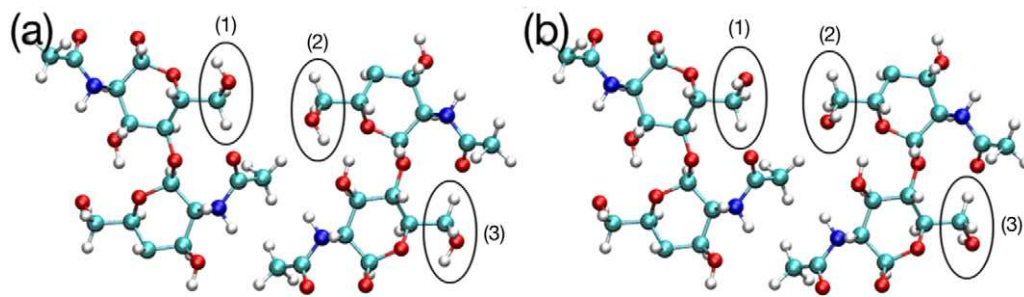


Fig. 5 – Ball and stick representation of α -chitin with highlighted hydroxymethyl $-\text{CH}_2\text{OH}$ side groups responsible for the conformational transition in Fig. 4(b). The hydroxymethyl side groups form rotational conformers (rotamers) which induce complex intra-molecular and inter-molecular hydrogen bond patterns. The geometries shown in (a) and (b) differ by a small expansion (smaller than 0.05 \AA) in the a lattice constant. The small change results in abrupt rotations of the hydroxymethyl groups, indicated as (1)–(3).

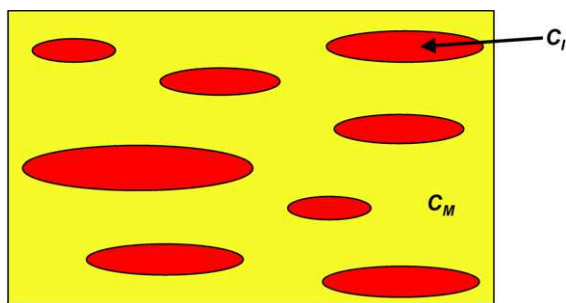


Fig. 6 – Schematic representation of an RVE related to the Mori-Tanaka model. C_I represents the stiffness tensor of the inclusions, C_M the stiffness tensor of the matrix.

(Fig. 2). Convenient engineering tools employed for the parameter transfer from a lower scale to an upper one are the homogenization methods explained next.

Let us consider a microscopically heterogeneous body and assume that it contains one dispersed phase (inclusions) embedded in a matrix phase (Fig. 6). Our objective is to predict the response of the entire composite body under given loads and boundary conditions based on its microstructure. To solve the problem one defines a representative volume element (RVE), which is generally much smaller than the studied body but is large enough to contain the same statistical information about the microstructure as the body itself and responds to given boundary conditions as a homogeneous piece of matter. Thus the goal of homogenization is to replace the heterogeneous RVE with a homogeneous material with the same averaged properties as the heterogeneous one.

One popular method to do this is mean-field homogenization, which is based on assumed relations between volume averages of stress or strain fields in each phase of the RVE. The simplest homogenization models are those of Voigt (uniform strain Voigt, 1889) and Reuss (uniform stress, Reuss, 1929). More sophisticated homogenization schemes are based on Eshelby's solution for a single ellipsoidal inclusion embedded in an infinite matrix (Eshelby, 1957). These models are limited to inclusions with ellipsoidal shape and use the following information about the microstructure: properties of each of the phases, corresponding volume fractions, shape (but not dimensions) and orientations of the inclusions.

A different homogenization approach has been developed by Torquato (1998, 2002). Besides the properties and the volume fractions of the phases, it is also designed to account for the specific arrangement of the inclusions. It consists of a series expansion approach containing a principal reference part and a fluctuation part (a perturbation about a homogeneous reference or comparison material), which contains three-point correlation functions that characterize the microstructure of the composite and its topology. The advantage of this method is that it is valid for arbitrary volume fractions of the inclusions and for arbitrary contrast between the mechanical properties of the phases.

2.3. Effective properties of chitin-protein fibers

At the atomistic scale, crystalline α -chitin exhibits a rather anisotropic character that respects the nature of the interatomic interactions which dominate along different directions. The response of chitin on stresses applied along the c -axis of the molecule is dominated by covalent bonds. Along the other two directions a hydrogen bond network is developed which is responsible for the cohesion of the anti-parallel atomic strings. The anisotropic character of the dominant interatomic interactions is clearly depicted in the energy-strain curves shown in Fig. 7. While the crystal response to deformations along the a and b directions is rather soft and of the same order of magnitude, the material is by nearly one order of magnitude stiffer along the c -axis. Thus, the anisotropy in the bonding character is expected to result in a highly anisotropic elastic matrix: the elastic constant which describes the elastic response of the material along the c -axis is by nearly one order of magnitude larger than the elastic constants governing the elastic properties of the bio-crystal along the other two directions. The shallow minimum appearing at $\sim 1\%$ tensile strain in the b lattice deformation profile denotes a metastable configuration of crystalline α -chitin, again highlighting the complex and flexible character of the hydrogen bond pattern.

With the obtained stiffness tensor of crystalline α -chitin, we derive the effective properties of a cluster of chitin-protein nanofibrils (Level III in Fig. 1) employing the above-described homogenization methods. The RVE of a single chitin-protein fiber (Level IIIa in Fig. 2) can be modeled as a composite

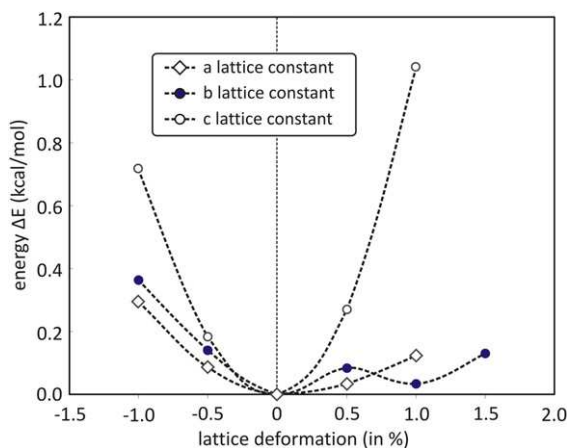


Fig. 7 – Theoretically determined total energy dependence as a function of the uniaxial strain for deformations along the three unit-cell vectors a , b , and c . The total energy of the global minimum is used as the reference energy. Positive (negative) values denote tensile (compressive) strain. The calculated data points are connected by the dashed line in order to guide the eye.

of aligned needle-like chitin nanofibrils embedded in an isotropic protein matrix.

The homogenized properties of such a single fiber depend on the properties of the chitin nanofibrils and the matrix proteins as well as on the shape and the volume fraction of the nanofibrils. It should be noted at this stage that the specific nanofibril and fiber arrangements, constituents, and shapes as represented in this model to form an RVE are specific for the lobster *H. americanus* and may vary for other arthropod species. The homogenized properties can now be derived by using the Mori–Tanaka homogenization scheme (Mori and Tanaka, 1973). It has been initially developed for two-phase composites reinforced with aligned ellipsoidal inclusions of the same shape (see Fig. 6) with relatively low volume fraction (not above 20–30% Torquato, 2002), i.e., there are no interactions between two neighboring inclusions. The Mori–Tanaka model for the effective properties of a composite fiber consisting of a certain volume of nanofibrils (here represented by the volume fractions and shapes of protein and chitin) can be written as (Benveniste, 1987)

$$\underline{C}_F = \underline{C}_{FP} + \phi_{CH}[(\underline{C}_{CH} - \underline{C}_{FP}) : \underline{A}_{CH}] [\phi_{FP} \underline{I} + \phi_{CH} \underline{A}_{CH}]^{-1}, \quad (1)$$

where

$$\underline{A}_{CH} = [\underline{I} + \underline{S}_{CH} : \underline{C}_{FP}^{-1} : (\underline{C}_{CH} - \underline{C}_{FP})]^{-1} \quad (2)$$

is the so-called strain concentration factor for an isolated single ellipsoidal inclusion in an infinite elastic matrix; \underline{C}_F , \underline{C}_{FP} and \underline{C}_{CH} denote the stiffness tensors of the homogenized fiber, the fiber proteins (matrix) and α -chitin (inclusions), respectively; \underline{I} is the fourth-order identity tensor, \underline{S}_{CH} is the fourth-order Eshelby's tensor depending only on the shape of the inclusions and on the elastic constants of the matrix; ϕ_{FP} and $\phi_{CH} = 1 - \phi_{FP}$ are the volume fractions of the protein matrix and the chitin crystallites, respectively. The tensor product contracted over two indices is denoted by (:), while

the inverse of a matrix (fourth-order tensors are represented in matrix notation because of symmetries) is indicated by $(\bullet)^{-1}$.

2.4. Twisted plywood (Bouligand) structure without canals

The RVE for a bulk twisted plywood structure without canals is schematically depicted in Fig. 2, Level IV. The elastic properties of the Bouligand structure are transverse isotropic, with symmetry axis along the cuticle normal. The simplest plywood with such properties consists of three identical plates reinforced with aligned chitin–protein fibers and rotated at 60° with respect to each other. The volume fraction of the aligned fibers in a single plate must be $\phi_F/3$ to match the fiber fraction in the whole RVE.

The effective properties of a single ply without canals can be found using the Mori–Tanaka method:

$$\underline{C}_P = \underline{C}_{MP} + \frac{\phi_F}{3} [(\underline{C}_F - \underline{C}_{MP}) : \underline{A}_F] \left[\left(1 - \frac{\phi_F}{3} \right) \underline{I} + \frac{\phi_F}{3} \underline{A}_F \right]^{-1}, \quad (3)$$

with strain concentration factor

$$\underline{A}_F = [\underline{I} + \underline{S}_F : \underline{C}_{MP}^{-1} : (\underline{C}_F - \underline{C}_{MP})]^{-1}, \quad (4)$$

where \underline{C}_P , \underline{C}_{MP} , and \underline{C}_F denote the stiffness tensors of the homogenized ply, the mineral–protein matrix, and the chitin–protein fibers, respectively; \underline{S}_F is the fourth-order Eshelby's tensor for a single chitin–protein fiber; ϕ_F is the volume fraction of the fibers in the whole RVE of the plywood.

Then the effective properties of the plywood can be found using the Voigt model assuming uniform strain in the plywood:

$$\underline{C}_{PW} = \frac{1}{3} \sum_{i=1}^3 \underline{R}_i^T : \underline{C}_P : \underline{R}_i,$$

where \underline{R}_i is a 6×6 rotation matrix constructed from the conventional 3×3 rotation matrix (see, e.g., Doghri, 2000) and the symbol $(\bullet)^T$ denotes the transpose of a matrix. The introduction of \underline{R}_i comes from the fact that the effective anisotropic properties for a given ply are found with respect to a local frame coinciding with the axes of symmetry of the ply fibers, and that frame in general does not coincide with the fixed coordinate system of the cuticle where the plywood stiffness \underline{C}_{PW} is defined.

2.5. Mineral–protein matrix

To solve Eqs. (3) and (4), we need the elastic constants \underline{C}_{MP} of the mineral–protein matrix (Fig. 2, Level IIIb). *In vivo*, the matrix consists of spherical ACC particles associated with proteins, and it possesses isotropic overall properties (Nikolov et al., 2010). Because the volume fraction of the ACC spheres is very high (about 70 wt% of the cuticle composition), we use the estimate developed by Torquato (1998) for isotropic two-phase composites where the dispersed phase is an array of spheres.

Let the indices 1 and 2 denote the matrix (proteins) and the dispersed phase (ACC spheres), respectively. Then, the effective three-dimensional (3D) shear modulus and bulk

modulus, G_e and k_e , of the composite are given by Torquato (1998)

$$G_e = G_1 \left[\frac{1 + \frac{9k_1 + 8G_1}{6(k_1 + 2G_1)} \mu \phi_2 - \frac{2\kappa \mu G_1}{3(k_1 + 2G_1)} \phi_1 \zeta_2 - \frac{\mu^2}{6} (F_\eta + F_\zeta)}{1 - \mu \phi_2 - \frac{2\kappa \mu G_1}{3(k_1 + 2G_1)} \phi_1 \zeta_2 - \frac{\mu^2}{6} (F_\eta + F_\zeta)} \right] \quad (5)$$

$$k_e = k_1 \left[\frac{1 + \frac{4G_1 \kappa \phi_2}{3k_1} - \frac{10\kappa \mu G_1}{3(k_1 + 2G_1)} \phi_1 \zeta_2}{1 - \kappa \phi_2 - \frac{10\kappa \mu G_1}{3(k_1 + 2G_1)} \phi_1 \zeta_2} \right], \quad (6)$$

where

$$F_\eta = \left[\frac{3k_1 + G_1}{k_1 + 2G_1} \right]^2 \phi_1 \eta_2; \quad F_\zeta = 5G_1 \left[\frac{2k_1 + 3G_1}{(k_1 + 2G_1)^2} \right] \phi_1 \zeta_2 \quad (7)$$

$$\kappa = \frac{k_2 - k_1}{k_2 + \frac{4G_1}{3}}; \quad \mu = \frac{G_2 - G_1}{G_2 + G_1} \frac{9k_1 + 8G_1}{6(k_1 + 2G_1)},$$

with G_1 and G_2 being the shear moduli and k_1 and k_2 the bulk moduli of the cuticle proteins and the ACC spheres, respectively; ϕ_1 and $\phi_2 = 1 - \phi_1$ represent the volume fractions of the proteins and of the mineral particles, respectively. The scalar parameters ξ_2 and η_2 are defined by three-fold integrals depending on the specific microstructure and on the volume fractions of the phases. With the obtained effective bulk and shear moduli, one can construct the stiffness tensor of the mineral–protein matrix, \underline{C}_{MP} .

2.6. Twisted plywood structure with pore canals

In a first approximation, the in-plane cross section of the cuticle with canals (Level V in Fig. 1) can be modeled as a regular honeycomb with thick walls. Having in mind that the cuticle has transverse isotropic properties, the twisted-ribbon shape of the ellipsoidal canals piercing the cuticle is approximated with hexagonal holes with straight walls and with the same cross-sectional area as the ellipsoidal openings in the cuticle. Thus, the main model parameter accounting for the pore canal system is the local area fraction of the canals. For the sake of simplicity, it is appropriate to consider the in-plane and the out-of-plane properties separately. In a plane perpendicular to the cuticle normal, for a two-dimensional (2D) sheet containing holes of arbitrary shape, the three-point approximations for the effective shear moduli and Young's moduli reduce to Hyun and Torquato (2000)

$$G_{CT} = \frac{k_{ST} G_{ST} \phi_S (\zeta + \eta - 1)}{(k_{ST} + 2G_{ST})(1 - \phi_S) + k_{ST}[1 - \phi_S(2 - \zeta - \eta)]} \quad (8)$$

$$E_{CT} = \frac{E_{ST} \phi_S (2\zeta - 1)(\zeta + \eta - 1)}{3 - 2\phi_S - 2(2 - \phi_S)(1 - \zeta) + (2 - \zeta - \eta)[2\phi_S(1 - \zeta) - 1]}, \quad (9)$$

where G_{CT} and G_{ST} are the in-plane shear moduli of the cuticle layer and of the plywood without canals, respectively; E_{CT} and E_{ST} are the in-plane Young's moduli of the cuticle and the plywood without canals, respectively; k_{ST} is the 2D in-plane bulk modulus of the solid cuticle tissue related to the 3D in-plane bulk modulus, K_{ST} , via $k_{ST} = 9K_{ST}G_{ST}/(3K_{ST} + 4G_{ST})$; ϕ_S denotes the area (or, equivalently, the volume) fraction of the solid; the scalar parameters ξ and η are defined by three-fold integrals depending on the shape and the arrangement of the holes and on the volume fractions of the phases. The

Poisson ratio of the cuticle in the transverse direction can be found from

$$\nu_{CT} = \frac{E_{CT}}{2G_{CT}} - 1. \quad (10)$$

In the normal direction of the cuticle, the Young's modulus, E_{CN} , and the Poisson ratio, ν_{CN} , can be expressed to a good approximation as (Christensen and Lo, 1979):

$$E_{CN} = \phi_S E_{SN}; \quad \nu_{CN} = \phi_S \nu_{SN}, \quad (11)$$

where E_{CN} and E_{SN} are the Young's moduli of the cuticle and the bulk plywood without canals in the normal direction, respectively; ν_{CN} and ν_{SN} stand for the Poisson ratios of the cuticle and the bulk plywood without canals in the normal direction, respectively. In Eq. (11), the Young's modulus and the Poisson ratio of the holes are taken to be zero.

Once the in-plane and out-of-plane Young's moduli and Poisson ratios of the twisted plywood with canals are calculated, we can compare them with the experimentally measured values and also reconstruct the 3D elastic constants of the cuticle.

3. Analysis of the biological design robustness and optimization

3.1. Reference simulations

The experimental data for the elastic properties of lobster cuticle are taken from Nikolov et al. (2010). The stiffness tensor of α -chitin obtained from *ab initio* calculations reads (Nikolov et al., 2010)

$$\underline{C}_{CH} = \begin{bmatrix} 119 & 0.1 & 1.1 & 0 & 0 & 0 \\ 0.1 & 28 & 2 & 0 & 0 & 0 \\ 1.1 & 2 & 24 & 0 & 0 & 0 \\ 0 & 0 & 0 & 5 & 0 & 0 \\ 0 & 0 & 0 & 0 & 8 & 0 \\ 0 & 0 & 0 & 0 & 0 & 2 \end{bmatrix} \text{GPa}. \quad (12)$$

It is defined in a local Cartesian coordinate frame where the vectors of the orthorhombic unit cell of α -chitin a , b and c (chain direction) are along the axes 2, 3 and 1, respectively.

For our reference simulations, the other model parameters are taken to be the same as in Nikolov et al. (2010).

The Young's modulus and Poisson ratio of the proteins within the chitin–protein fibers are 4 MPa and 0.49, respectively. The Young's modulus and the Poisson ratio of the ACC spherules are 37 GPa and 0.35, respectively, and those of the proteins in the mineral–protein matrix have been identified as 1.2 GPa and 0.45, respectively. The volume fraction of the chitin–protein fibers in the mineral–protein matrix, ϕ_F , is 0.2, while that of chitin within a single chitin–protein fiber is $\phi_{CH} = 0.17$. The average area fraction of the canal openings in the cuticle is $\phi_C = 0.3$. The corresponding statistical parameters for the honeycomb properties in Eqs. (9), (10) are $\eta = 0.93$ and $\zeta = 0.97$.

The arrangement of the ACC spherules is assumed to form a symmetric cell material. In Nikolov et al. (2010), we tested three different hypotheses for the possible microstructure of the mineral–protein matrix: (i) overlapping spheres;

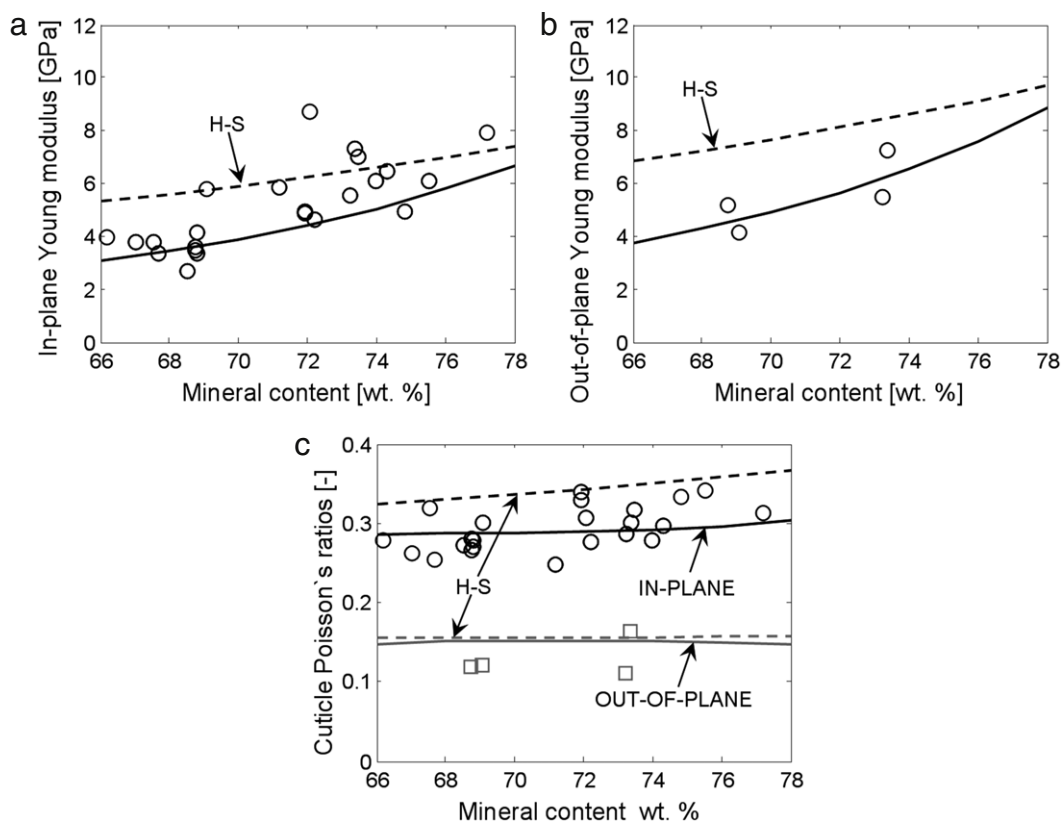


Fig. 8 – (a) In-plane Young's modulus versus mineral content. (b) Out-of-plane Young's modulus versus mineral content. (c) Cuticle in-plane and out-of-plane Poisson ratios versus mineral content. Symbols: experimental data (Nikolov et al., 2010); solid lines: model predictions. The dashed lines H-S are obtained when the mineral–protein matrix attains the upper Hashin–Strikman bound.

(ii) random array of impenetrable spheres with polydispersity in size; and (iii) symmetric cell material with spherical cells. Other arrangements are not possible because for high mineralization grades the measured volume fraction of ACC spherules exceeds the theoretical packing density. It has been shown that the assumption of symmetric cell material explains the observed material behavior much better than the other possible arrangements.

We note that a symmetric cell material is defined by the following procedure. First, the space is divided into spherical cells with different diameters so that their sizes are distributed in a statistically homogeneous and isotropic manner throughout the material. Then to each cell the property of the mineral (with probability ϕ) or protein (with probability $1 - \phi$) is assigned randomly and independently from the properties of the other cells so that the volume fraction ϕ of the spheres has the property of the mineral and the volume fraction $1 - \phi$ has the property of the protein. The resulting composite is macroscopically homogeneous and isotropic.

With the above-mentioned parameters, we perform reference simulations for the cuticle's elastic properties as a function of the mineral content (Fig. 8). In addition we redo the simulations when the mineral–protein matrix has elastic properties equal to the upper Hashin–Strikman bound that cannot be exceeded by any composite material.

Fig. 8(a) shows that the in-plane cuticle modulus is fairly close to the Hashin–Strikman bound. Some experimental points are even beyond this bound. We believe that this is due to experimental shortcomings and possibly because our model slightly underestimates the in-plane modulus owing to the somewhat simplifying assumption of a regular honeycomb structure of the cuticle instead of the complex twisting canal system with elliptical openings. The out-of-plane modulus (Fig. 8(b)) is strictly below the H–S bound and is well predicted by the simulation as well as the two Poisson ratios depicted in Fig. 8(c). Based on these results, one may speculate that, during mineralization, small fractions of the mineral–protein matrix may actually form a Hashin–Strikman assembly of coated spheres while most of the ACC spheres adopt the structure of symmetric cell material.

3.2. Influence of the properties of chitin–protein fibers on the macroscopic behavior

3.2.1. Elastic constants of α -chitin

To estimate the sensitivity of the overall cuticle properties to variations in the properties of the chitin–protein fibers, we first consider the α -chitin elastic constants. We vary the reference values of each of the three largest elastic constants (C_{11} , C_{22} , C_{33}) in Eq. (12) by $\pm 50\%$.

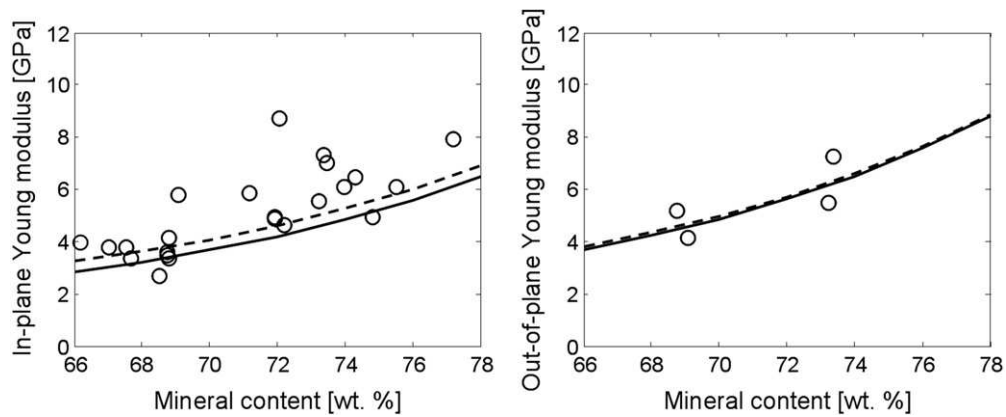


Fig. 9 – Influence of different C_{11} values on the elastic moduli of the cuticle. Dashed lines: $1.5C_{11}$; solid lines: $0.5C_{11}$ ($C_{11} = 119$ GPa). Symbols: experimental data.

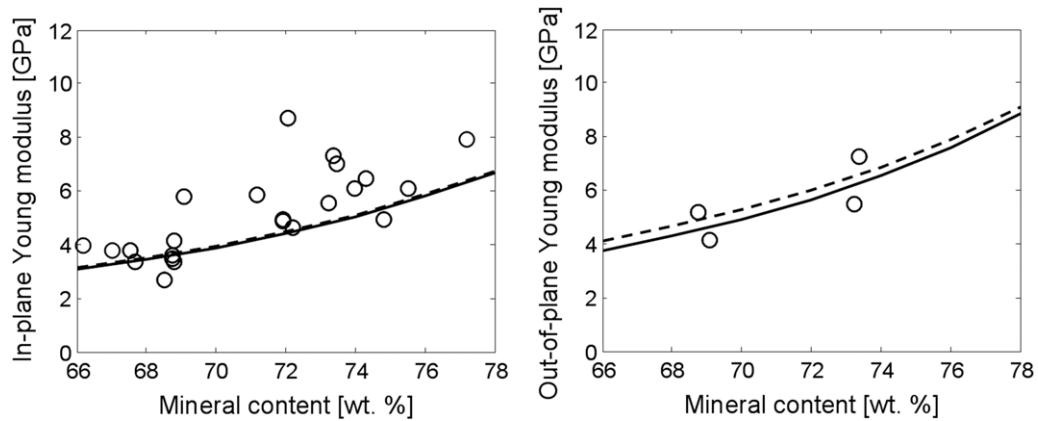


Fig. 10 – Influence of different values for Young's modulus of the fiber proteins. Dashed lines: $E_p = 40$ MPa; solid lines: $E_p = 4$ MPa; symbols: experimental data (E_p : Young's modulus of the fiber proteins).

Fig. 9 reveals that the (significant) variation of the largest elastic constant of chitin C_{11} (along the chain direction) influences the cuticle in-plane modulus only moderately and practically does not change the out-of-plane modulus, which is plausible. The variations of the two other large constants, C_{22} and C_{33} , have negligible influence on the behavior. For these cases, the curves obtained for the moduli are basically indistinguishable, and we do not show them here.

In conclusion, the particular elastic constants of chitin have little (in the case of C_{11}) or no influence (for all others) on the overall behavior of the cuticle. This is due to the very low volume fraction of chitin in the tissue (only about 4%) and to the very strong contrast between the elastic moduli of chitin and the fiber proteins (4 MPa), which reduces the composite fiber moduli considerably compared to those of pure chitin.

3.2.2. Young's modulus of fiber proteins

Next we consider the influence of the value of the Young's modulus of the fiber proteins, which has been identified as 4 MPa based on experiments with unmineralized lobster joint membranes containing chitin (Sachs, 2008). We set this value one order of magnitude higher, to 40 MPa, and compare the result with the reference simulation in Fig. 10.

The results in Fig. 10 show that much stiffer fiber proteins would slightly increase the out-of-plane cuticle modulus because in long fiber composites with stiff fibers the matrix influences the transverse properties more, while the macroscopic in-plane modulus remains virtually unchanged because the fibers are oriented in the cuticle plane and their behavior is dominated by the stiff covalent longitudinal direction of the chitin. Again we observe that significant variations in the properties of the fiber constituents have little effect on the cuticle performance.

3.2.3. Volume fraction of α -chitin in the fibers

Finally, we vary the volume fraction of the chitin crystallites in a chitin-protein fiber within the experimentally observed bounds. The chitin nanofibrils have a polygonal cross section with effective diameter of about 3 nm and length of about 300 nm (Neville et al., 1976). They are separated from each other at distances ranging from 3 to 5 nm and are arranged in quasi-hexagonal packing (Giraud-Guille, 1990). The volume fraction, ϕ_{CH} , of the chitin nanofibrils is geometrically modeled as cylindrical fibers with hexagonal packing according to

$$\phi_{CH} = \frac{2\pi R_f^2}{\sqrt{3}(2R_f + s)^2},$$

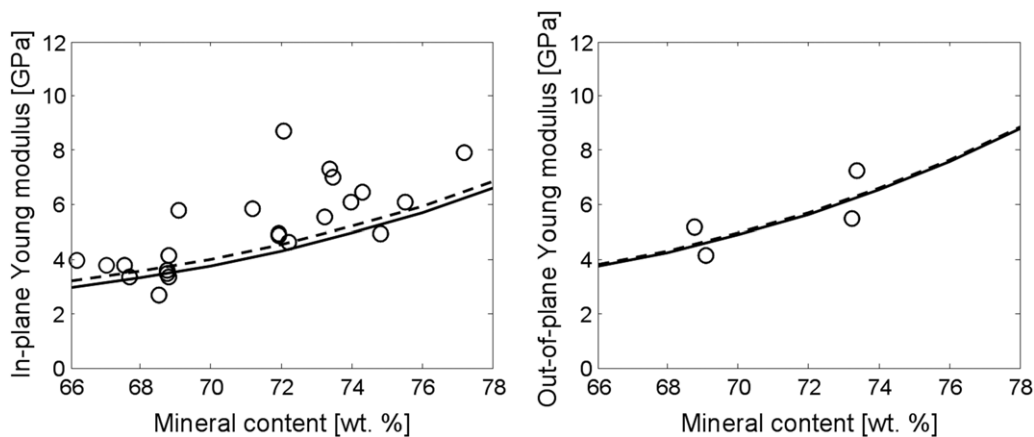


Fig. 11 – Influence of the volume fraction of chitin in the fibers on the macroscopic moduli. Dashed lines: $\phi_{CH} = 0.23$; solid lines: $\phi_{CH} = 0.13$; symbols: experimental data. ϕ_{CH} : volume fraction of chitin.

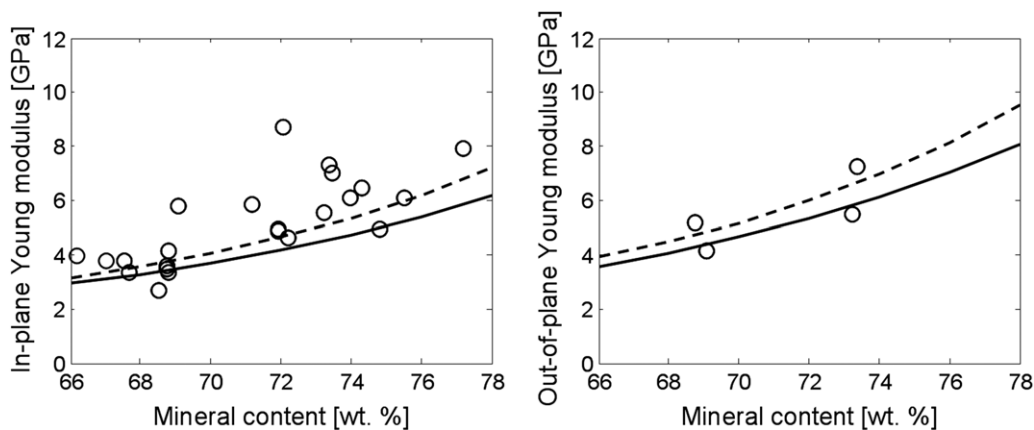


Fig. 12 – Influence of the ACC modulus on the macroscopic moduli. Dashed lines: $E_{ACC} = 40.7$ GPa; solid lines: $E_{ACC} = 33.3$ GPa; symbols: experimental data. E_{ACC} : Young's modulus of the hard ACC phase.

where R_f and s denote the fiber radius and the lateral separation between them, respectively. For the uniform separation distances between the chitin crystallites of 3 and 5 nm, the corresponding volume fractions of chitin, ϕ_{CH} , are 0.13 and 0.23, respectively. We perform simulations with these limiting values leaving the other model parameters as reference ones; see Fig. 11.

Fig. 11 shows that the most likely variations of the volume fraction of chitin in the fibers have little effect on the in-plane modulus and do not change the out-of-plane modulus.

In conclusion, we observe that the overall properties of the cuticle are extremely robust to large variations in the properties and the volume fractions of the fiber constituents (chitin and fiber proteins), which not only have low volume fractions in the cuticle tissue but are also related to a lower hierarchy level in the cuticle structure.

3.3. Influence of the properties of the mineral–protein matrix

3.3.1. Young's modulus of the ACC spherules

Clearly, an important reason for the robustness of the overall cuticle properties with respect to the properties of the

chitin–protein fibers is that the fibers represent only 20% of the volume of the bulk tissue. To ensure a more relevant comparison of the influence of the properties of the mineral–protein matrix components on the macroscopic behavior, we scale down the variations imposed to the fiber constituents by multiplying them by the fiber volume fraction (0.2). Thus the Young's modulus of the hard ACC phase (37 GPa) is varied by $\pm 10\%$. The result of this variation is shown in Fig. 12.

Fig. 12 reveals that the cuticle properties are more sensitive to variations in the ACC modulus, given that ACC forms from 66 to 78 wt% of the cuticle. Still, the difference in the elastic moduli even for a mineral content of 78 wt% (15%) is less than the imposed variation of the moduli (20%).

3.3.2. Young's modulus of the ACC matrix proteins

In our simulations, the Young's modulus of the ACC matrix proteins are identified as 1.2 GPa based on our simulations. In fact, experimentally, nothing is known about the mechanical properties of these proteins. We apply the same procedure as for the ACC modulus and decrease the Young's modulus two times compared to the tenfold increase in the fiber protein modulus. The asymmetric variations of the proteins moduli

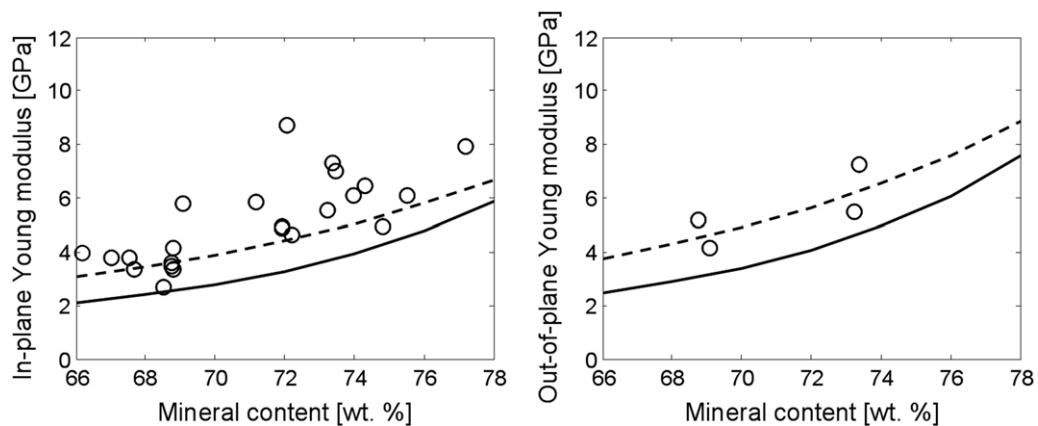


Fig. 13 – Influence of the modulus of proteins in the ACC matrix on the macroscopic moduli. Dashed lines: $E_{MP} = 1200$ MPa; solid lines: $E_{MP} = 600$ MPa; symbols: experimental data. E_{MP} : Young's modulus of the ACC matrix proteins.

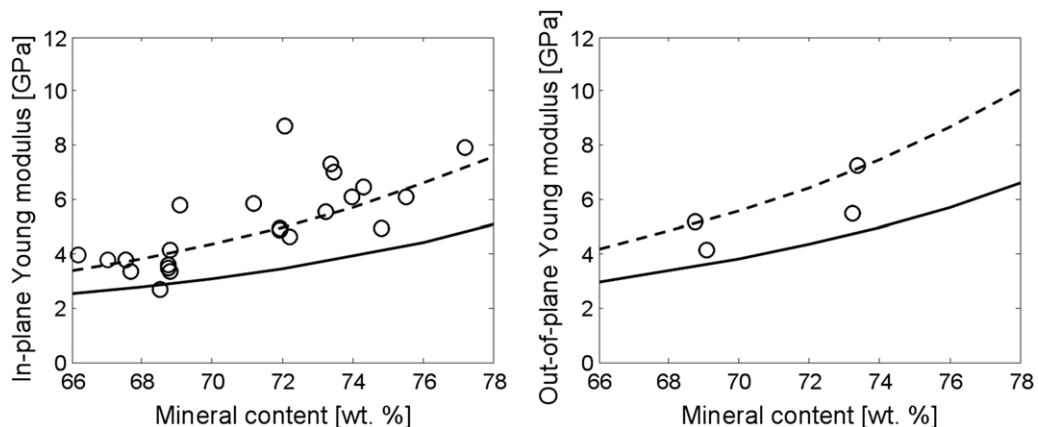


Fig. 14 – Influence of the volume fraction of the chitin-protein fibers, ϕ_F , on the macroscopic cuticle moduli. Dashed lines: $\phi_F = 0.23$; solid lines: $\phi_F = 0.13$; symbols: experimental data. ϕ_F : volume fraction of fibers in the ACC matrix.

are justified by the fact that 4 MPa for the modulus of the fiber proteins is a realistic value but is at the lower end of the known moduli for proteins, while 1.2 GPa for the matrix proteins is at the higher end of the known protein moduli; see Fig. 13.

Fig. 13 reveals that the variations in the Young's modulus of the matrix proteins by 100% lead to significant variations of the cuticle moduli given that the volume fraction of the ACC matrix proteins in the cuticle is small.

3.4. Influence of the volume fraction of chitin-protein fibers in the ACC-protein matrix

The chitin-protein fibers in lobster cuticle have a diameter of about 20 nm. The average separation between individual fibers has not been measured experimentally. For the formation of biominerals, a minimum spacing of 20 nm is required (Bouligand, 1972). Assuming a separation between the fibers of 20 nm and hexagonal packing, we obtain an upper limit for the volume fraction of fibers in the ACC matrix as $\phi_F = 0.23$. For the lower limit, we choose $\phi_F = 0.13$ (the same as for chitin in the fibers), which corresponds to a separation of about 35 nm; see Fig. 14.

Fig. 14 shows that variations of $\sim 75\%$ in the local volume fraction of the chitin-protein fibers lead to roughly the same percentage variations of the macroscopic cuticle moduli. Thus we identify the local volume fraction of the chitin-protein fibers as one of the critical design parameters of the cuticle, together with the mineral content and the pore canals area fraction. Optimal (higher) fiber volume fraction results in optimal macroscopic properties of the cuticle.

3.5. Best-case and worst-case accumulative scenarios for the elastic stiffness

Next we consider best-case and worst-case scenarios for the elastic cuticle properties (Fig. 15). The best-case scenario is obtained by applying simultaneously the above-mentioned variations in the properties and the volume fractions of the cuticle constituents that maximize the elastic moduli. Correspondingly the worst-case situation is obtained by applying all considered variations that minimize the moduli of the intermediate constituents and thus also of the overall modulus. Here we do not vary the area of the canal pore openings (this has been considered in Nikolov et al. (2010)) and concentrate instead on the bulk tissue properties.

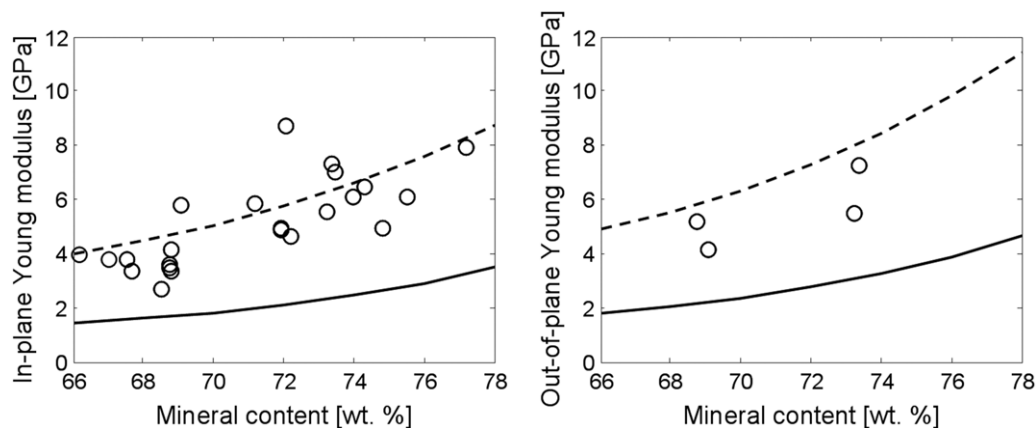


Fig. 15 – Best-case (dashed, upper curve) and worst-case (solid, lower curve) scenarios obtained with accumulative changes that maximize (dashed)/minimize (solid) the elastic overall moduli. It is most remarkable that the experimentally observed modulus results (open symbols) are close to the best-case theoretical scenario; i.e., the hierarchical organization of the material provides an optimal use of the properties of the underlying ingredients.

Fig. 15 shows the best-case (dashed, upper curve) and worst-case (solid, lower curve) scenarios obtained with accumulative changes that maximize (dashed) or, respectively, minimize (solid) the elastic overall moduli. Interestingly, the analysis reveals that the experimentally observed cuticle properties correspond much better to the best-case scenario than to the worst-case one. This result suggests that the specific hierarchical structure of the lobster cuticle leads to an optimal use of the stiffness of the individual ingredients; i.e., the cuticle design apparently exploits the full potential of its underlying ingredients. On the other hand, the use of elastically softer components and lower than optimal volume fractions of the main structural units leads to a significant deterioration in the overall elastic properties of the cuticle.

In order to better understand the design principles behind the excellent cuticle properties, Fig. 16 shows the characteristic Young's moduli of some key load-bearing structural components versus their characteristic size in double logarithmic presentation, in part also emphasizing their elastic anisotropy. Similar upper–lower bound scale-dependent design charts have been proposed by Lahaie et al. (1995) for the strength of metallic composites, which were in turn based on earlier work of Ashby (1993). These earlier size-dependent composite charts apply to elastic–plastic loading of metals, while biological materials are typically optimized with respect to optimal elasticity (not plasticity). In a linear elasticity composite, the properties essentially follow a linear rule of volumetric mixture. Hence, in the current case, the main observation is not in the first place the size dependence of the elastic modulus which is obtained through the hierarchical structure evolution from small to large size but the fact that the extreme anisotropy of the chitin nanofibrils is rendered into an isotropic material through this arrangement. This reflects a very general principle in the construction of chitin-based cuticles that, in terms of topology, represents 'structural increase in dimensions' from smaller to larger length scales. The chitin nanofibrils, a quasi-1D object, self-assemble in quasi-2D chitin–protein planes (Fig. 1, level V),

which in turn form a cholesteric liquid crystal-like 3D structure (twisted plywood).

Fig. 17 shows a 3D Ashby map that also involves the mineral volume fraction. It is interesting that the overall mineralization is such that the modulus of the mineral–protein matrix at very high mineralization grades is similar to the axial modulus of the chitin protein fibers. Further mineralization would yield a matrix that is stiffer than the stiffest fiber direction, which would not make a better composite, and hence is not realized.

3.6. Summary

To summarize and better analyze our results, we introduce a sensitivity measure similar to that defined in Reisinger et al. (2010) and list the sensitivity of the in-plane macroscopic Young's modulus $E^{\text{in-plane}}$ of the cuticle with respect to variations in the constituent properties and volume fractions at different hierarchy levels in Table 1. The sensitivity measure is defined as

$$S = \frac{\partial E^{\text{in-plane}}}{\partial X} \approx \frac{\Delta E^{\text{in-plane}}}{\Delta X}, \quad (13)$$

where X is a constituent property (e.g., Young's modulus) or volume fraction. An obvious drawback of such a measure is that it has different units for different kinds of variable; for example, it is unitless or is measured in GPa when X represents a Young's modulus or volume fraction, respectively. Still, it allows us to compare separately the sensitivity to variations in the elastic properties of the constituents on the one hand, and volume fractions on the other. Except for the sensitivity to the overall mineral content, all other estimates are for a typical mineral content of 70 wt% (0.51 ACC volume fraction).

From Table 1, one can see that, as far as volume fractions are concerned, the in-plane cuticle modulus is most sensitive to the overall mineral content and the volume fraction of the chitin protein fibers (Levels IIIa and IV in Fig. 2). Surprisingly, the cuticle properties are more sensitive to the Young's modulus of the matrix proteins than to the calcium carbonate modulus.

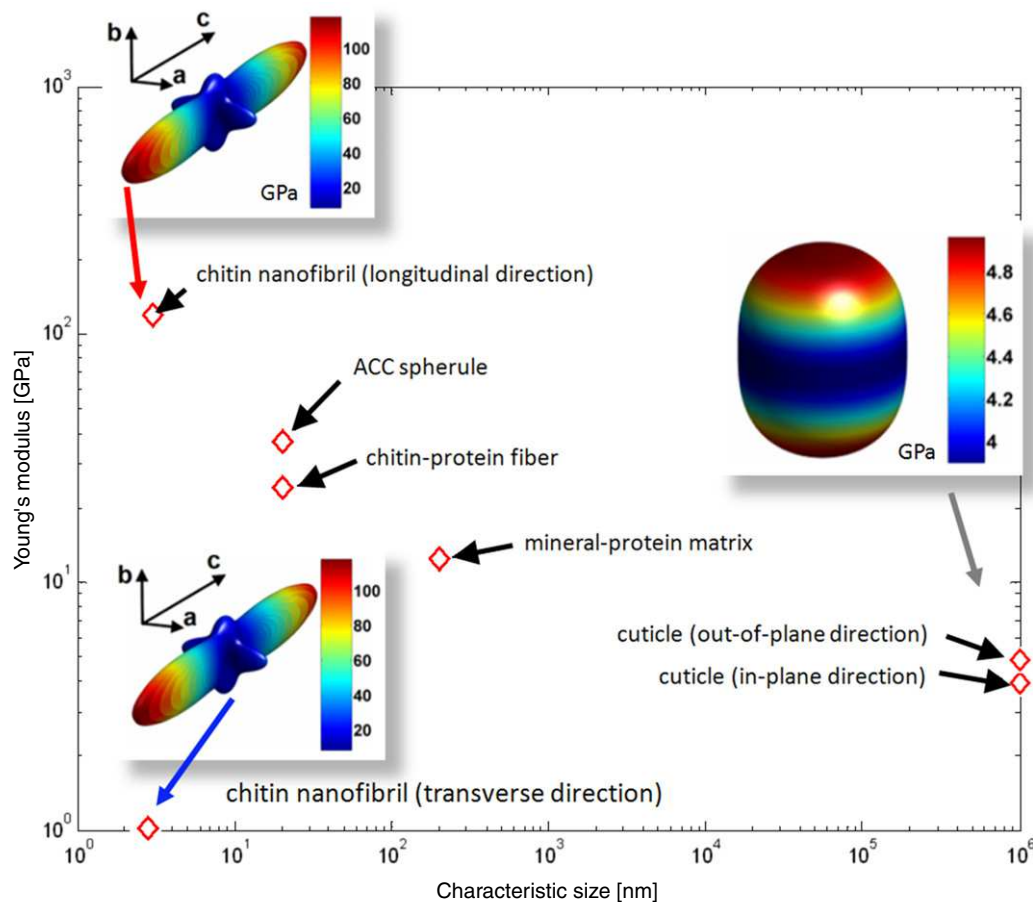


Fig. 16 – Scale-dependent design chart for the elastic modulus of load-bearing structural units of the lobster cuticle at a typical mineralization grade of 70 wt%, placing particular attention on the relationship between size and elastic anisotropy.

4. Discussion and conclusions

Using a multiscale modeling approach that links the atomistic to the continuum scale, we have shown that lobster cuticle and, quite possibly, many other biological nanocomposites, possess excellent mechanical properties close to the theoretical upper Hashin–Strikman bound of mechanical behavior.

In general, one can consider the robustness of the cuticle behavior with respect to variations or error propagation as coming from four different sources: hierarchy level, properties of the constituents of specific structure at this level, geometric design parameters such as volume fractions, and the structure itself (e.g., that of symmetric cell material). Regarding the key structures appearing at lower hierarchy levels, this study shows that the cuticle macroscopic behavior appears to be very robust with respect to large variations in the properties of chitin–protein fibers owing to the specific hierarchical structure and the huge contrast in the properties of chitin and fiber proteins. The cuticle response is somewhat more sensitive to variations in the constituent properties of the mineral–protein matrix (ACC and matrix proteins), and very sensitive to the specific (symmetric cell material) structure of the mineral–protein matrix and the overall mineral content (Nikolov et al., 2010). At higher hierarchy levels, some geometric design parameters such as the volume

fraction of the chitin–protein fibers play a very important role in the cuticle performance, and the sensitivity of the cuticle behavior to such parameters is significant. We also observe that, among the possible variations in the cuticle ingredients and volume fractions, the experimental data reflect an optimal use of the structural variations regarding the best possible performance for a given composition. It seems that the smart hierarchical organization of the cuticle design leads to an optimal use of the stiffness of the individual ingredients.

The present approach can be applied to other hierarchical biomaterials without limitations as long as the proper homogenization models are used for each hierarchy level beyond the atomistic scale. A purely continuum version of this approach has been developed to study the elasticity of a mineralized collagen fibril array and the role of extrafibrillar mineralization in bone (Nikolov and Raabe, 2008).

Our analysis is limited to the elastic properties in the small-deformation regime. At large deformations, where yield, damage and failure strength are major issues, certain nanoscale features that have little influence at small strains may become a determining factor of the cuticle mechanical behavior. For example, findings in studies of genetic disease in soft collagen tissue show a significant impact of nanoscale features such as crosslink density (Buehler, 2008) or single amino acid mutations (Gautieri et al., 2009) on the small-strain and especially on the large-strain mechanical behavior.

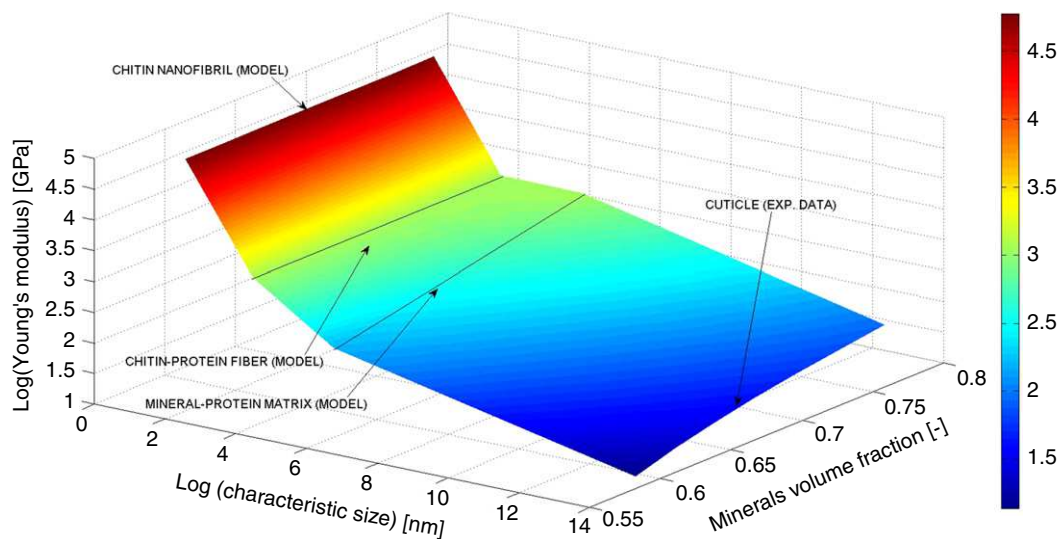


Fig. 17 – 3D Ashby map of the Young's modulus containing the size scale dependence and the mineral volume fraction.

Table 1 – Estimated sensitivity of $E^{\text{in-plane}}$ to variations in the elastic properties and the volume fractions of key structural components of the cuticle.

Constituent property (volume fraction)	Hierarchy level (Figs. 1, 2)	Sensitivity S w.r.t. $E^{\text{in-plane}}$ (GPa)	Units of S
$C_{11\alpha}$ -chitin (GPa)	I, II	0.0037	–
E_p fiber proteins (GPa)	II	~0	–
Vol. fraction α -chitin (-)	IIIa	2.2	GPa
E_{ACC} (GPa)	IIIb	0.06	–
E_{MP} matrix proteins (GPa)	IIIb	1.67	–
Mineral content (-)	IIIb	28.57	GPa
ϕ_F chitin-protein fibers (-)	IV	14.4	GPa

At present, we have investigated the large-strain behavior of mineralized cuticle only experimentally (e.g., Romano et al., 2007; Sachs et al., 2008; Sachs, 2008; Fabritius et al., 2009). The numerical simulation and analysis of the nonlinear cuticle response using a physically based multiscale model is the subject of future work.

Acknowledgements

The authors gratefully acknowledge the financial support through the Gottfried-Wilhelm-Leibniz Program and through the DFG priority program SPP 1420, both funded by the Deutsche Forschungsgemeinschaft (German Research Foundation).

REFERENCES

Al-Sawalmih, A., Li, C., Siegel, S., Fabritius, H., Yi, S.B., Raabe, D., Fratzl, P., Paris, O., 2008. Microtexture and chitin/calcite orientation relationship in the mineralized exoskeleton of the American lobster. *Adv. Funct. Mater.* 18, 3307–3314.
 Ashby, M.F., 1993. Criteria for selecting the components of composite. *Acta Metall. Mater.* 41, 1313–1335.
 Ashby, M.F., Wegst, U.G.K., 2004. The mechanical efficiency of natural materials. *Phil. Mag.* 84, 2167–2181.

Benveniste, Y., 1987. A new approach to the application of Mori-Tanaka's theory in composite materials. *Mech. Mater.* 6, 147–157.
 Boßelmann, F., Romano, P., Fabritius, H., Raabe, D., Epple, M., 2007. The composition of the exoskeleton of two crustacea: the American lobster *Homarus americanus* and the edible crab *Cancer pagurus*. *Thermochim. Acta* 463, 65–68.
 Bouligand, Y., 1972. Twisted fibrous arrangements in biological materials and cholesteric mesophases. *Tissue Cell* 4, 189–217.
 Buehler, M.J., 2008. Nanomechanics of collagen fibrils under varying cross-link densities: atomistic and continuum studies. *J. Mech. Behav. Biomed. Mater.* 1, 59–67.
 Buehler, M.J., Wong, S.Y., 2007. Entropic elasticity controls nanomechanics of single tropocollagen molecules. *Biophys. J.* 93, 37–43.
 Carlström, D., 1957. The crystal structure of α -chitin. *J. Biophys. Biochem. Cytol.* 3, 669–683.
 Chen, P.-Y., Lin, A.Y.-M., Stokes, A.G., Seki, Y., Bodde, S.G., McKittrick, J., Meyers, M.A., 2008. Structural biological materials: overview of current research. *JOM* 60, 23–32.
 Christensen, R.M., Lo, K.H., 1979. Solutions for effective shear properties in three phase sphere and cylinder models. *J. Mech. Phys. Solids* 27 (4), 315–330.
 Currey, J.D., 1996. Biocomposites: micromechanics of biological hard tissue. *Curr. Opin. Solid State Mater. Sci.* 1, 440–445.
 Doghri, I., 2000. *Mechanics of Deformable Solids: Linear and Nonlinear, Analytical and Computational Aspects*. Springer, Berlin.
 Elstner, M., 2006. The SCC-DFTB method and its application to biological systems. *Theor. Chem. Acc.* 116, 316–325.

- Eshelby, J.D., 1957. The determination of the elastic field of an ellipsoidal inclusion, and related problems. *Proc. R. Soc. Lond. Ser. A* 241, 376–396.
- Fabritius, H., Sachs, C., Romano, P., Raabe, D., 2009. Influence of structural principles on the mechanics of a biological fiber based composite material with hierarchical organization: the exoskeleton of the lobster *H. americanus*. *Adv. Mater.* 21, 391–400.
- Fratzl, P., Weinkamer, R., 2007. Nature's hierarchical materials. *Prog. Mater. Sci.* 52, 1263–1334.
- Gautieri, A., Uzel, S., Vesentini, S., Redaelli, A., Buehler, M.J., 2009. Molecular and mesoscale mechanisms of osteogenesis imperfecta disease in collagen fibrils. *Biophys. J.* 97 (3), 857–865.
- Giraud-Guille, M.-M., 1990. Chitin crystals in arthropod cuticles revealed by diffraction contrast transmission electron microscopy. *J. Struct. Biol.* 103, 232–240.
- Hild, S., Marti, O., Ziegler, A., 2008. Spatial distribution of calcite and amorphous calcium carbonate in the cuticle of the terrestrial crustaceans *Porcellio scaber* and *Armadillidium vulgare*. *J. Struct. Biol.* 163, 100–108.
- Hild, S., Neues, F., Žnidaršič, N., Štrus, J., Epple, M., Marti, O., Ziegler, A., 2009. Ultrastructure and mineral distribution in the tergal cuticle of the terrestrial isopod *Titanethes albus*. Adaptations to a karst cave biotope. *J. Struct. Biol.* 168, 426–436.
- Hohenberg, P., Kohn, W., 1964. Inhomogeneous electron gas. *Phys. Rev. B* 136, 864.
- Hyun, S., Torquato, S., 2000. Effective elastic and transport properties of regular honeycomb structures for all densities. *J. Mater. Res.* 15, 1985–1993.
- Jensen, F., 1999. *Introduction to Computational Chemistry*. John Wiley & Sons, Inc., USA.
- Kohn, W., Sham, L.J., 1965. Self-consistent equations including exchange and correlation effects. *Phys. Rev. A* 140, 1133.
- Lahaie, D.J., Embury, J.D., Ashby, M.F., 1995. Scale dependent composite design charts. *Scr. Metall. Mater.* 32, 133–138.
- Lotmar, W., Picken, L.E.R., 1950. A new crystallographic modification of chitin and its distribution. *Experientia* 6, 58.
- Merzendorfer, H., 2006. Insect chitin synthases: a review. *J. Comp. Physiol. B* 176, 1–15.
- Meyers, M.A., Chen, P.-Y., Lin, A.Y.-M., Seki, Y., 2008. Biological materials: structure and mechanical properties. *Prog. Mater. Sci.* 53, 1–206.
- Minke, R., Backwell, J., 1978. Structure of α -chitin. *J. Mol. Biol.* 120, 167–181.
- Monkhorst, H.J., Pack, J.D., 1976. Special points for Brillouin-zone integrations. *Phys. Rev. B* 13, 5188.
- Mori, T., Tanaka, K., 1973. Average stress in matrix and average elastic energy of materials with misfitting inclusions. *Acta Metall.* 21, 571–574.
- Nardi, F., Wade, R.C., 1999. Ways and means to enhance the configurational sampling of small peptides in aqueous solution in molecular dynamics simulations. In: Balbuena, P.B., Seminario, J.M. (Eds.), *Molecular Dynamics; From Classical to Quantum Methods*. Elsevier, New York, pp. 859–898.
- Neues, F., Ziegler, A., Epple, M., 2009. The composition of the mineralized cuticle in marine and terrestrial isopods: a comparative study. *Cryst. Eng. Comm.* 9, 1245–1251.
- Neville, A.C., Parry, D.A., Woodhead-Galloway, J., 1976. The chitin crystallite in arthropod cuticle. *J. Cell Sci.* 21 (1), 73–82.
- Nikolov, S., Petrov, M., Lymperakis, L., Friák, M., Sachs, C., Fabritius, H.-O., Raabe, D., Neugebauer, J., 2010. Revealing the design principles of high-performance biological composites using ab initio and multiscale simulations: the example of lobster cuticle. *Adv. Mater.* 22, 519–526.
- Nikolov, S., Raabe, D., 2008. Hierarchical modeling of the elastic properties of bone at submicron scales: the role of extrafibrillar mineralization. *Biophys. J.* 94, 4220–4232.
- Ortiz, C., Boyce, M.C., 2008. Bioinspired structural materials. *Science* 319, 1053–1054.
- Perdew, J.P., Burke, K., Ernzerhof, M., 1996. Generalized gradient approximation made simple. *Phys. Rev. Lett.* 77, 3865–3868.
- Raabe, D., Romano, P., Sachs, C., Fabritius, H., Al-Sawalmih, A., Yi, S.-B., Servos, G., Hartwig, H.G., 2006. Microstructure and crystallographic texture of the chitin–protein network in the biological composite material of the exoskeleton of the lobster *H. americanus*. *Mater. Sci. Eng. A* 421, 143–153.
- Raabe, D., Sachs, C., Romano, P., 2005. The crustacean exoskeleton as an example of a structurally and mechanically graded biological nanocomposite material. *Acta Mater.* 53, 4281–4292.
- Rapp, A.K., Casewit, C.J., Colwell, K.S., Goddard, W.A., Skiff, W.M., 1992. UFF, a full periodic table force field for molecular mechanics and molecular dynamics simulations. *J. Am. Chem. Soc.* 114, 10024–10039.
- Reisinger, A.G., Pahr, D.H., Zysset, P.K., 2010. Sensitivity analysis and parametric study of elastic properties of an unidirectional mineralized bone fibril-array using mean field methods. *Biomech. Model. Mechanobiol.* doi:10.1007/s10237-010-0190-1.
- Reuss, A., 1929. Berechnung der Fließgrenze von Mischkristallen auf Grund der Plastizitätsbedingung für Einkristalle. *Z. Angew. Math. Mech.* 9, 49–58.
- Rinaudo, M., 2006. Chitin and chitosan: properties and applications. *Prog. Polym. Sci.* 31, 603–632.
- Romano, P., Fabritius, H., Raabe, D., 2007. The exoskeleton of the lobster *H. americanus* as an example of a smart anisotropic biological material. *Acta Biomater.* 3, 301–309.
- Sachs, C., 2008. Microstructure and mechanical properties of the exoskeleton of the lobster *H. americanus* as an example of a biological composite material. Ph.D. Thesis. RWTH Aachen.
- Sachs, C., Fabritius, H., Raabe, D., 2006. Hardness and elastic properties of dehydrated cuticle from the lobster *H. americanus* obtained by nanoindentation. *J. Mater. Res.* 21, 1987–1995.
- Sachs, C., Fabritius, H., Raabe, D., 2008. Influence of microstructure on deformation anisotropy of mineralized cuticle from the lobster *H. americanus*. *J. Struct. Biol.* 161, 120–132.
- Tai, K., Dao, M., Suresh, S., Palazoglu, A., Ortiz, C., 2007. Nanoscale heterogeneity promotes energy dissipation in bone. *Nat. Mater.* 6, 454–462.
- Tang, H., Buehler, M.J., Moran, B.A., 2009. Constitutive model of soft tissue: from nanoscale collagen to tissue continuum. *Ann. Biomed. Eng.* 37 (6), 1117–1130.
- Torquato, S., 1998. Effective stiffness tensor of composite media: II. Applications to isotropic dispersions. *J. Mech. Phys. Solids* 35, 1411–1440.
- Torquato, S., 2002. *Random Heterogeneous Materials: Microstructure and Macroscopic Properties*. Springer, New York.
- Troullier, N., Martins, J.L., 1991. Efficient pseudopotentials for plane-wave calculations. *Phys. Rev. B* 43, 1993.
- Vincent, J.F.V., 1990. *Structural Biomaterials*. Princeton University Press, USA.
- Vincent, J.F.V., Wegst, U.G.K., 2004. Design and mechanical properties of insect cuticle. *Arthropod Struct. Dev.* 33, 187–199.
- Voigt, W., 1889. Über die Beziehung zwischen den beiden Elastizitätskonstanten isotroper Körper. *Wied. Ann.* 38, 573–587.
- Weiner, S., Addadi, L., 1997. Design strategies in mineralized biological materials. *J. Mater. Chem.* 7, 689–702.